Research Article

Xin Nie*, Chi Zhang, Chenchen Wang, Shichang Nie, Jie Zhang, and Chaomo Zhang

Variable secondary porosity modeling of carbonate rocks based on μ-CT images

https://doi.org/10.1515/geo-2019-0049
Received Dec 05, 2018; accepted Aug 27, 2019

Abstract: As an essential carbonate reservoir parameter, porosity is closely related to rock properties. Digital rock physics (DRP) technology can help us to build forward models and find out the relationship between porosity and physical properties. In order to prepare models for the rock physical simulations of carbonate rocks, digital rock models with different porosities and fractures are needed. Based on a three-dimensional carbonate digital rock image obtained by X-ray microtomography (μ-CT), we used erosion and dilation in mathematical morphology to modify the pores, and fractional Brownian motion model (FBM) to create fractures with different width and angles. The pores become larger after the erosion operation and become smaller after the dilation operation. Therefore, a series of models with different porosities are obtained. From the analysis of the rock models, we found out that the erosion operation is similar to the corrosion process in carbonate rocks. The dilation operation can be used to restore the matrix of the late stages. In both processes, the pore numbers decrease because of the pore surface area decreases. The porosity-permeability relation of the models is a power exponential function similar to the experimental results. The structuring element B's radius can affect the operation results. The FBM fracturing method has been proved reliable in sandstones, and because it is based on mathematics, the usage of it can also be workable in carbonate rocks. We can also use the processes and workflows introduced in this paper in carbonate digital rocks reconstructed in other ways. The models we built in this research lay the foundation of the next step physical simulations.

Keywords: carbonate, digital rock physics, secondary porosity, fracture, mathematical morphology, fractional Brownian motion

1 Introduction

Approximately 50% of oil and gas are stored in carbonate rocks around the world. Porosity is one of the critical parameters for reservoir evaluation. Unlike typical sandstone reservoirs with single-porosity systems, reservoirs in carbonate rocks commonly have multiple-porosity systems which cause petrophysical heterogeneity [1]. Porosity in carbonate rocks can be classified based on the timing of porosity evolution into primary pores and secondary pores [2]. Primary porosity includes pores supported by the particles when sediments were depositing. Secondary porosity includes pores form as a result of post-depositional dissolution. There are also natural fractures in carbonates. Due to the complexity of carbonate rock pore space, it's difficult to carry out the petrophysical interpretation for predicting the transport properties and producibility of carbonate reservoirs [3].

To evaluate the pore properties, first work we need to do is forward modeling which reveals the relationship between porosity and physical properties. The digital rock physics (DRP) technology has been helpful in the forward modeling in sandstones [4–8], carbonates [3], natural gas reservoirs [9], fractured rocks [10], thinly bedded rocks [11], and shales [12, 13] in recent years. With DRP, rock physical properties such as elastic moduli [14], acoustic properties [15], electrical properties [16], and fluid flow properties [17]. The digital rock models with different porosities are needed in the simulations. Arns *et al.* (2005) [3] characterized the carbonates in a pore-scale using X-ray mi-

***Corresponding Author: Xin Nie:** Key Laboratory of Exploration Technologies for Oil and Gas Resources, Yangtze University, Wuhan, Hubei 430100, China; Cooperative Innovation Center of Unconventional Oil and Gas, Yangtze University, Wuhan 430100, China; Email: niexin_cugb@126.com

Chi Zhang: University of Kansas, KS 66045, United States of America

Chenchen Wang: Cooperative Innovation Center of Unconventional Oil and Gas, Yangtze University, Wuhan 430100, China; iRock Technologies, Beijing 100094, China

Shichang Nie, Jie Zhang: Key Laboratory of Exploration Technologies for Oil and Gas Resources, Yangtze University, Wuhan, Hubei 430100, China

Chaomo Zhang: Key Laboratory of Exploration Technologies for Oil and Gas Resources, Yangtze University, Wuhan, Hubei 430100, China; Cooperative Innovation Center of Unconventional Oil and Gas, Yangtze University, Wuhan 430100, China

crotomography (μ-CT) which is an accurate way to build a digital rock model. However, for a single rock sample, the porosity is fixed. Therefore, lots of rock samples need to be scanned to build rock models with different porosities. First, it isn't economic to scan so many samples; second, for different carbonate rocks, the secondary porosities formed in the diagenesis are different, which causes the trend of simulation results not so visible. Other mathematical methods have been used to generate models with different porosities, including stochastic methods [18, 19] and process-based methods [20], etc. There are too many uncertainties using these stochastic methods. Recently, many studies have been done to simulate the CO2 injection, and numerical study of carbonate dissolution by CO2 and its effect on the transport properties are presented [21–25]. These process-based methods can provide us accurate models with different porosities after the present dissolution stage. However, the stages before present still cannot be acquired. Therefore, to get more models of the stages before present, we introduce dilation and erosion in mathematical morphology to process the μ-CT scanned carbonate rock image. We also introduce the application of fractional Brownian motion algorithm (FBM) to generate natural fractures in μ-CT scanned images in carbonate rock to get fractured models.

2 Methodology

2.1 Dilation and erosion in mathematical morphology

Mathematical morphology is a standard method used in image processing. The principle of mathematical morphology method is to use a structure element with a specific shape to measure and pick up the equal shape in the image to analyze the image. There are four basic operation modes: dilation, erosion, opening, and closing [26]. The opening and closing operations have been used on sandstones to generate fluid distributions in the pore space [27].

In mathematical morphology, dilation operation and erosion operation are opposite processes. The dilation operation enlarges the target image, while the erosion operation reduces the target image. The mathematical morphology is based on set theory. Sets in mathematical morphology represent the shapes which are manifested on binary or gray tone images. A and B are two sets; $A \oplus B$ means the dilation of A by B, while $A \ominus B$ means the erosion of A by B. Eq. 1 and 2 are expressions of dilation and erosion,

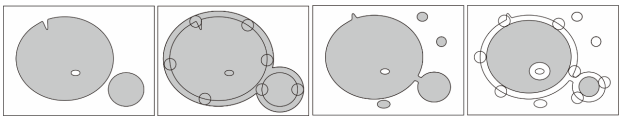

(a) Original image M (b) Dilation of M by B (c) Original image N (d) Erosion of N by B

Figure 1: Sketch of dilation and erosion

respectively.

$$A \oplus B = \{x \,|B_x \cap A \neq \emptyset\} \tag{1}$$

$$A \ominus B = \{x \,|B_x \subseteq A\} \tag{2}$$

In Eq. 1 and 2, B_x is the translations of set B by x; $\emptyset$ is null. Figure 1 is a 2D sketch of dilation and erosion. Figure 1(a) shows an original image M. In this case, B is a disc with a fixed radius, and the origin is the center of the circle. After the dilation of M by B, the image $M \oplus B$ is as the grey part shown in Figure 1(b). The original image is enlarged with a certain radius outward. Figure 1(c) is another original image N. The grey part shown in Figure 1(d) is $N \ominus B$, *i.e.* the erosion of image N by B. In this case, M and N are images, and B is structuring element. In our study, we use a sphere structuring element for 3D processing.

2.2 Fractional Brownian motion

Experimental evidence [28] shows that the roughness of natural fracture internal surfaces in rocks follows self-affine fractal statistics. In this paper, we adopt the idea of considering a rock surface without overhangs. The surface height is described by a function $h(x, y)$, with the coordinates x and y lying in the mean plane of the fracture [10]. Self-affinity of the rough surfaces implies scale invariance. When $x \rightarrow \lambda_x x$, $y \rightarrow \lambda_y y$, $h \rightarrow \lambda_h h$, we assume that $\lambda_x = \lambda_y = \lambda$ and $\lambda_h = \lambda_H$, and then we have the following equation:

$$h(x, y) = \lambda^{-H} h(\lambda x, \lambda y) \tag{3}$$

where λ is the scale factor, H is the roughness (Hurst exponent). For the surfaces of fractures presented in rocks, the roughness exponent is around H = 0.8, which has no relationship with the lithology and fracture mode [29].

Fractional Brownian motion (FBM) is a standard mathematical model for self-affine fractals, which fits the following equation:

$$E\left[\left(G_H(X + h) - G_H(X)\right)^2\right] = |h|^{2H}\sigma^2, (0 < H < 1) \tag{4}$$

where $G_H(X)$ is a random walking which satisfies the Fractional Brownian motion; E is mathematical expectation; H

is the roughness exponent; σ is standard deviation; σ_0 is a random initial standard deviation between 0~1; j is the times of iterative operations.

According to central-limit theorem, Eq. (4) can be written as:

$$\sigma^2(h) = \sigma^2(1)h^{2H} \tag{5}$$

standard deviation σ can be calculated as follow equation:

$$\sigma^2{}_j = \frac{\sigma^2{}_{j-1}}{2^H} = \frac{\sigma^2{}_0}{(2^H)^j}\left(1 - \frac{2^H}{4}\right) \tag{6}$$

There are many algorithms to generate FBM data. In this paper, we adopt a corrected successive random addition (CSRA) algorithm to generate the FBM surfaces [30, 31].

The workflow of this algorithm for 2D square surface is as follows (Figure 2):

(1) First select random numbers from and add them to the 4 corner points of the square, denoted by number 1, where stands for a Gaussian random number generator with a mean of 0 and a variance σ_0^2.
(2) Calculate the midpoint denoted by number 2 by linear interpolation based on the 4 corner point values.
(3) Select random numbers from (σ_1^2 can be derived from Eq. (6)) and add them to all the existing points;
(4) Calculate the midpoints on each side of the square denoted by number 3 by linear interpolation using two adjacent corner values obtained in step 3;
(5) Select random numbers from $N(0\sigma_2^2)$ (σ_2^2 can be derived from Eq. (6)) and add them to all existing points.
(6) Repeat the process, keep performing linear interpolations and adding random numbers from $N(0\sigma_j^2)$ up to the nth level, resulting in a total of $(2^n+1)^2$ points. Then the generation of the 2D rough surface is done (*e.g.*, Figure 3).

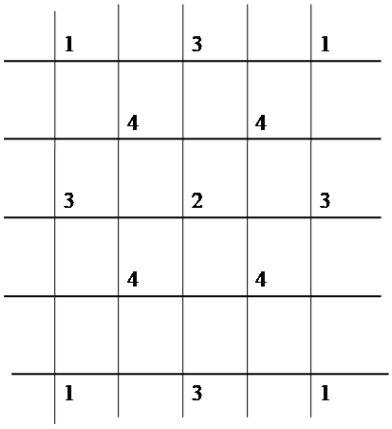

Figure 2: Point denoting and value assignment order of SRA

Figure 3: Rough surface created by using SRA algorithm

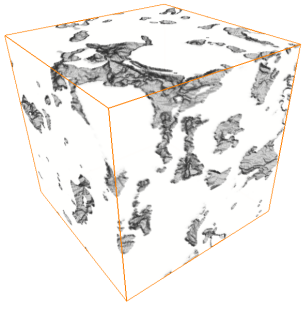

Figure 4: The μ-CT scanned digital rock sample C1 of carbonate rock used in this study

3 Carbonate rock secondary porosity modeling results

3.1 μ-CT based 3D digital rock

In this study, we use a 3D image of a carbonate rock (named C1) obtained using Microcomputed X-ray tomography (μ-CT) from Imperial College London [32]. The segmented 3D carbonate digital image is shown in Figure 4, which has 400×400×400 voxels. The resolution is 2.85μm/voxel, and the porosity is 17.6%.

3.2 Modeling of carbonate digital rock with different porosities

One most important component of carbonate reservoir pore space is secondary porosity formed by corrosion. Corrosion process in the carbonate rocks is similar to the erosion operation in mathematical morphology. Therefore, we use erosion to mimic the later stages in a corrosion process. Based on the digital rock model obtained by μ-CT scanning and using the erosion operation, we generated the digital carbonate rocks with different porosities.

Figure 5 shows an example result of digital carbonate rocks with different porosities after the erosion. In these digital rocks, pixels with value 0 (shown as black parts)

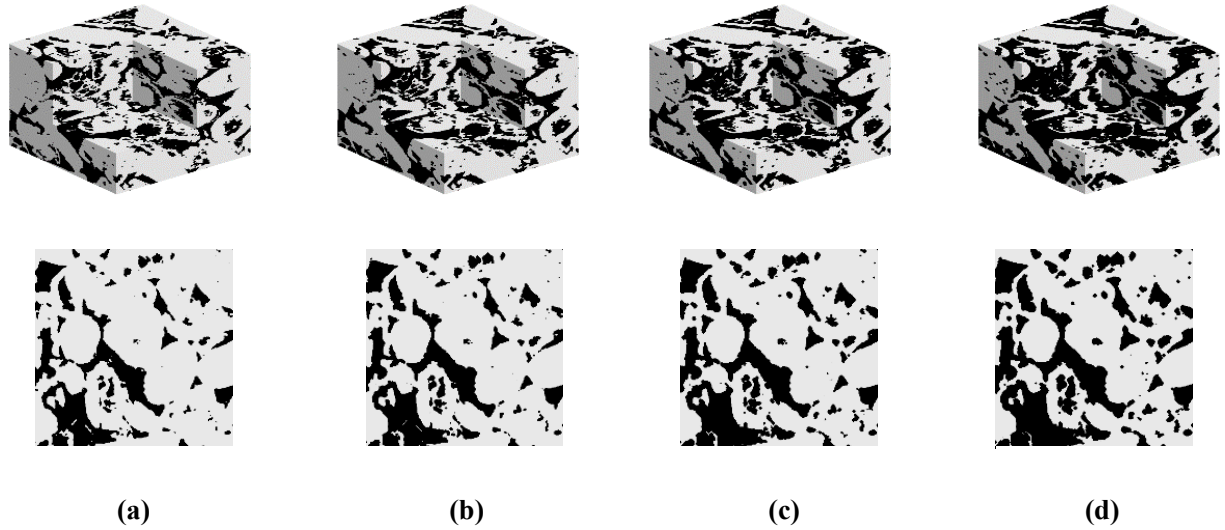

Figure 5: Digital rocks and their slices of carbonates with different porosities generated after the erosion process. (a) Original image (Φ= 23.26%); (b) Image after 1 erosion (Φ = 29.22%); (c) Image after 2 erosion (Φ= 34.93%); (d) Image after 3 erosion (Φ = 40.4%)

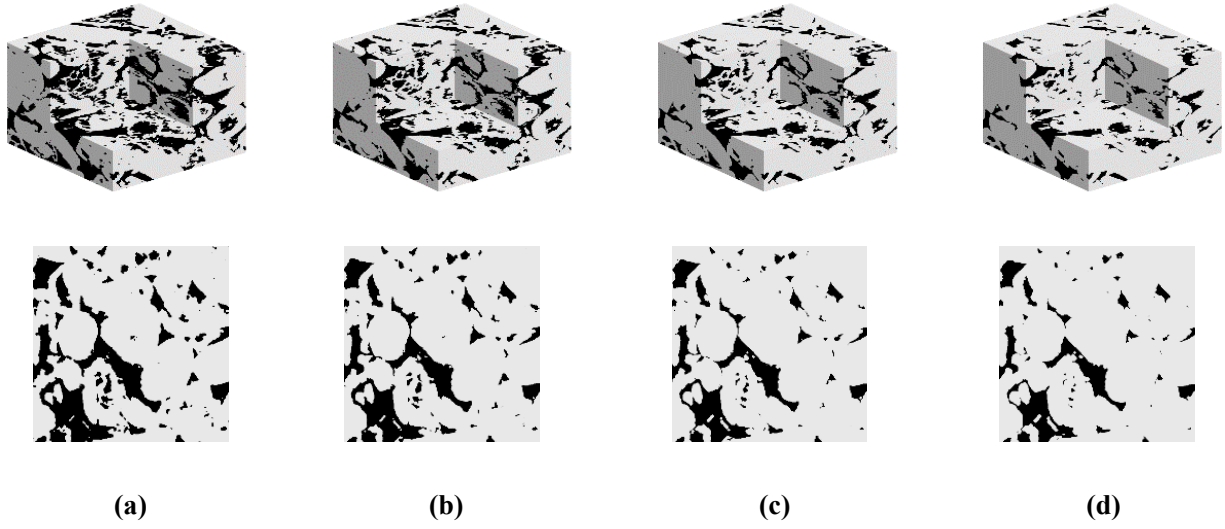

Figure 6: Digital rocks and their slices of carbonates with different porosities generated afterdilation process. (a) Original image (Φ= 23.26%); (b) Image after 1 dilation (Φ= 17.76%); (c) Image after 2 dilation (Φ= 13.5%); (d) Image after 3 dilation (Φ= 10.22%)

represent pore space, while those with value 1 (shown as lighter parts) represent the matrix. The structuring element is a sphere with a radius of 1 pixel. Figure 5a is the original core and its one slice, and Figure 5b~d is the cores and their slices after 1~3 times of erosion. As we can see in Figure 5, after the sphere goes around the pore space, the matrix is eroded, resulting in an increase of porosity. And during the process, pores used to be close to each other can merge as one larger pore. Through this way, we can increase the porosity of the carbonate digital rock models.

With the erosion, we generated digital rocks with higher porosities. Meanwhile, by using the dilation process to dilate the matrix, digital rocks with lower porosities can be acquired. The structuring element is the same as in the erosion process. Figure 6 shows the dilation results. Figure 6a is the original core and its one slice, and Figure 6b~d is the cores and their slices after 1~3 times of dilation. As we can see in Figure 6, after the sphere goes around the pore space, the matrix is dilated, resulting in a decrease of porosity. Some small pore space vanishes into the matrix. This process can be seen as reverse of a corrosion process. The cores with lower porosities can be seen as earlier stages of the corrosion process. Through this way,

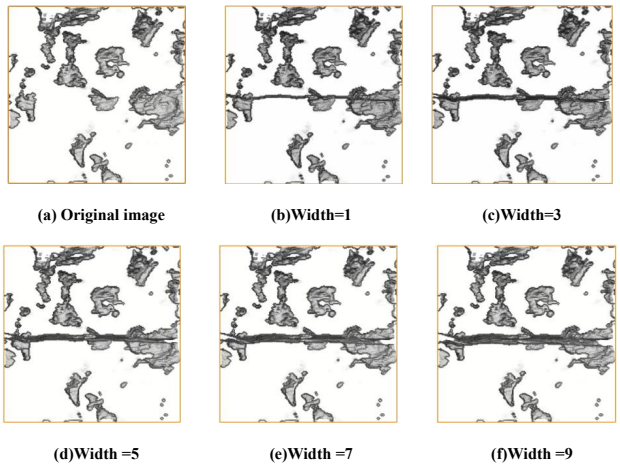

Figure 7: Sections of fractured carbonate digital rock models with different fracture widths

we can decrease the porosity of the carbonate digital rock models.

3.3 Modeling of fractured rocks

Fractures are another critical space for carbonate reservoirs. They can be both reservoir space and seepage channels. But due to the difficulty in coring and doing experiments for fractured formations, the research about fractured carbonate reservoirs hasn't been well done before. Digital rock technology can be introduced to provide fractured rock models which can be the basis of numerical simulations. In this study, we use fBm to generate fractures with different widths and angles.

For a digital rock with 400×400×400 voxels, we choose a 400×400 pixels area in the rough surface $z=f(x,y)$ generated by using FBM in Section 2. Then we set it as the lower surface of the fracture. Set the width of the fracture as d, then the upper surface $Z=z+d$. Because 0 represents pore space, we set the pixels between upper and lower surfaces as 0. By changing the value of d, we can get different fracture widths. By setting the pixels where the fractures are supposed to be as 0 in the original image, we can obtain the digital rock models with fractures different in widths (*e.g.*, Figure 7).

According to the attitudes of the fractures, they can be divided into "high angle" (dip angle > 75°), "bevel" (15° < dip angle < 75°) and "low angle" (dip angle < 15°) fractures. To mimic different attitudes, by rotating the fractures, we can obtain fractured digital rocks with varying angles of dip (*e.g.*, Figure 8).

4 Discussion

4.1 Pore geometry, numbers and porosity changes of models after erosion and dilation

Because the secondary corrosion pore space in carbonate rocks is formed through the corrosion process which is similar to dilation and erosion operations in mathematical morphology, the dilation and erosion processes are adopted in this research to simulate different stages of eroded pores. Our goal is to have variable porosity but retain a similar pore structure. Therefore, we use the maximal ball algorithm [32] to extract the pore network (Figure 9) and statistic the pore and throat numbers of all radiuses. The balls and sticks in Figure 9 represent pores and throats, respectively, and different colors show different pore sizes. From blue to red, the pore size increases.

From the network models, the pore/throat radius distribution curves of the digital rock models with different porosities can be obtained (Figure 10). In Figure 10, the frequency in y-axis stands for the count of the radius in x-axis divided by the whole count. C11~C15 are the names of digital rock models after erosion, and C1_1~C1_7 are the ones after dilation. As we can see in Figure 10, the peak of the curve slightly shifts right in the erosion process, while it moves left in the dilation process. This reveals the pores are somewhat enlarged or shrunken during the respective operations.

The numbers of pores are counted (Figure 11). In Figure 11, each dot represents a dilation or erosion processing point. In both processes of erosion and dilation, the pore numbers decrease. This also indicates that in the dilation process, the small pores vanish; and in the erosion process, the nearby pores merge into bigger ones. Figure 12 shows the porosity change rate during the operations. As we can see in Figure 12, the more the processes have been done, the slower the erosion and dilation process is. Because each process only adds on or peels off a fixed thickness of one voxel on the pore surface, the speed of change relates only to the surface area. As a result of small pores vanishing or nearby pores merging, the pore surface decreases in both processes.

4.2 Porosity-permeability relation

The relationship between porosity and permeability is always concerned by petroleum engineers and petrophysicists. Many studies reveal that in on a particular area or

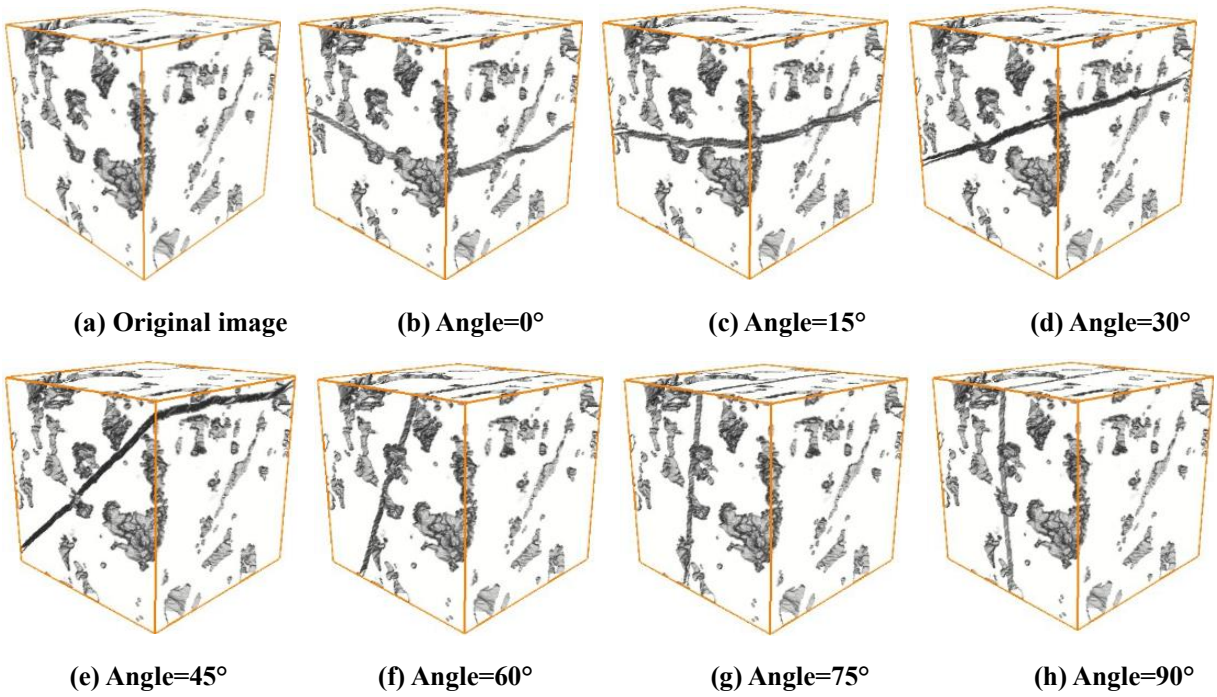

Figure 8: Models of fractured carbonate digital rock models with different fracture angles

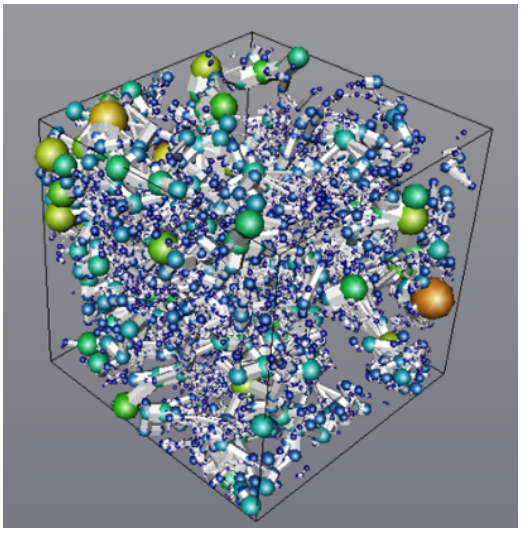

Figure 9: Pore network of C1 digital rock model

for one specific kind of carbonate, the permeability can be a power function of porosity (*e.g.*, Rashid *et al.*, 2015). We have some carbonate rock samples with laboratory experimental permeability results (Figure 13). The trend is also power exponential. As we can see, there are rock samples with minimal porosity and high permeability. This reveals there might be micro-fractures in those samples. Based on the network models, the permeabilities of the digital rock models are calculated by using the single-phase flow permeability calculation method based on Darcy's law [34]. The simulation results are shown in Figure 14. As we can see in Figure 14, the trend is similar to the experimental results of carbonate rock samples from a specific area acquired in the laboratory. Because the simulations are based on the same sample, the trend of the simulation results is more evident than the laboratory results. This indicates the method used to modify the porosity in this paper is reasonable. The models can be used in the next-step physical simulations.

4.3 The effect of *B*'s radius on porosity changing

In this study, we adopt a sphere with a radius of 1 voxel as the structuring element *B*. The porosity changes by one layer of voxel on the pore surface during each process. Because the resolution of this 3D digital rock is 2.85μm/voxel, the pores' radiuses change 2.85μm (by add or minus) each time. In a pixel image, processing with the sphere structuring elements with different radius can cause different results. We compare the dilation and erosion results of the digital rock by a sphere with a radius of one voxel for five times and by a sphere with a radius of five voxels for one time. The statistic results are shown in Table 1. C13 and C1_3 are the results of erosion and dilation by *B* with a

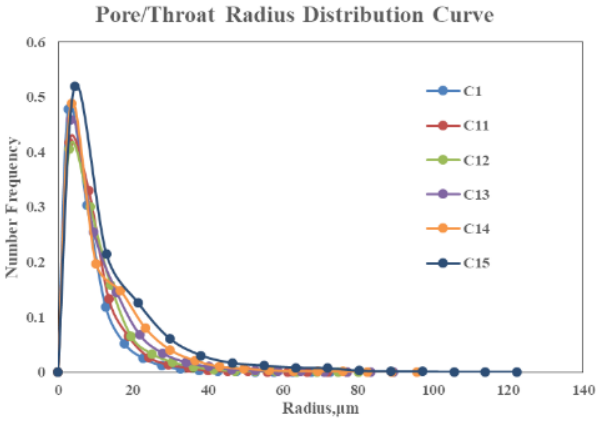

(a) Erosion results

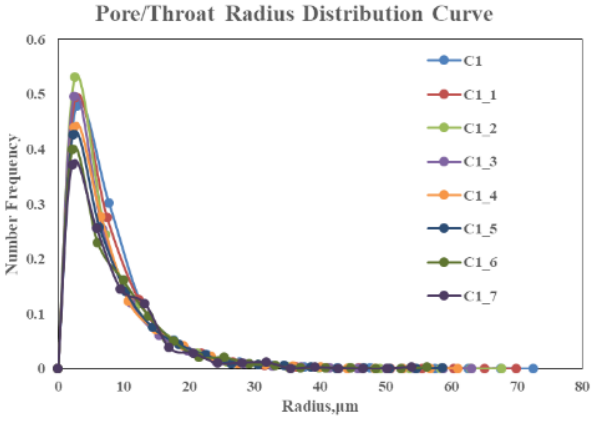

(b) Dilation results

Figure 10: Pore/throat radius distribution curves of the digital rock models

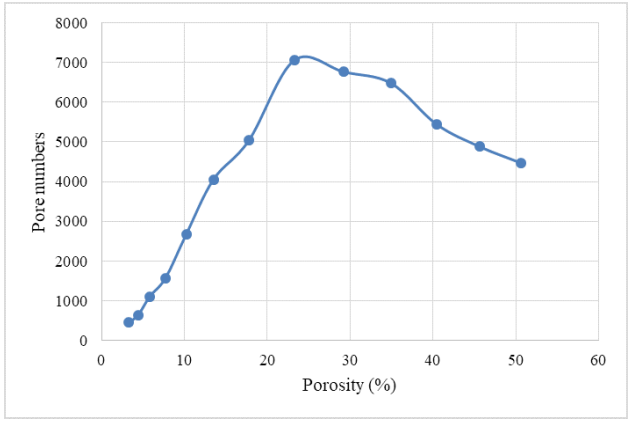

Figure 11: Pore numbers of digital rocks with different porosities

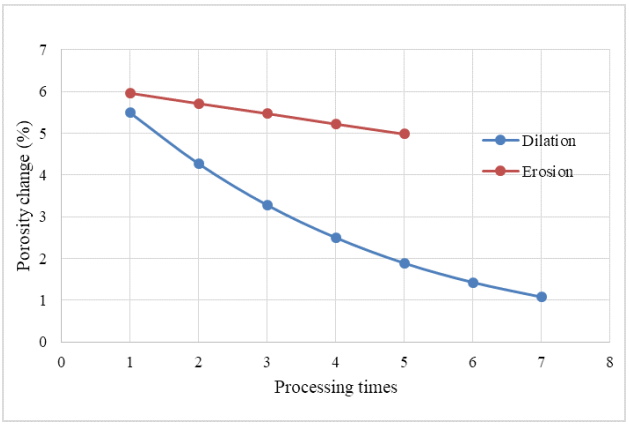

Figure 12: Porosity change variation with the processing times

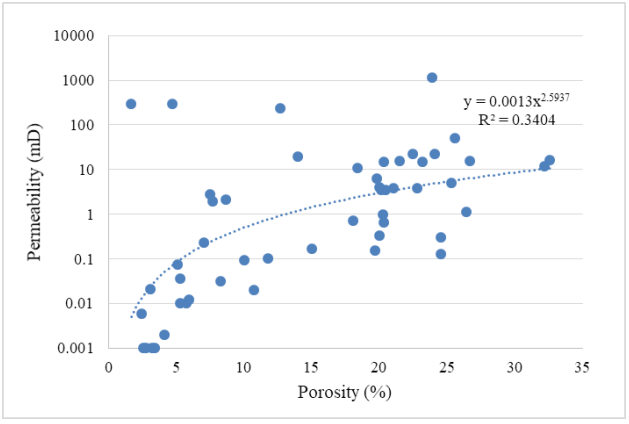

Figure 13: Laboratory experimental permeability results of carbonate rock samples

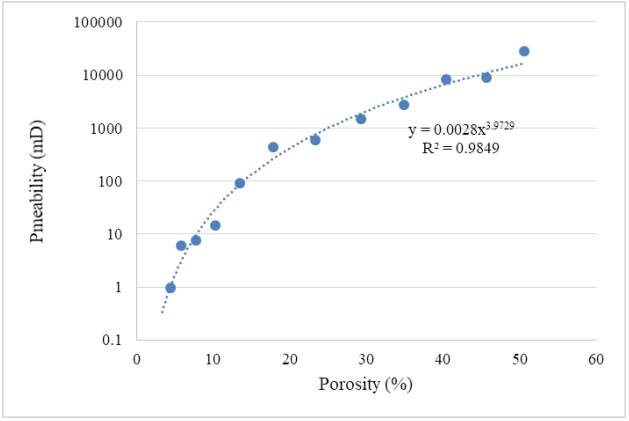

Figure 14: Permeability simulation results of the models generated after erosion and dilation

radius of one voxel for three times, and C13r and C1_3r are the ones by B with a radius of three voxels for one time. There are differences in porosity, permeability, and pore numbers. The porosity and permeability change more when B's radius is three voxels than one voxel. Figure 15 shows the pore networks of the four digital rocks. From the network images, we can see some differences in pore connection. In the dilation process, when B's radius is three voxels, the smaller throats and pores are less. This makes

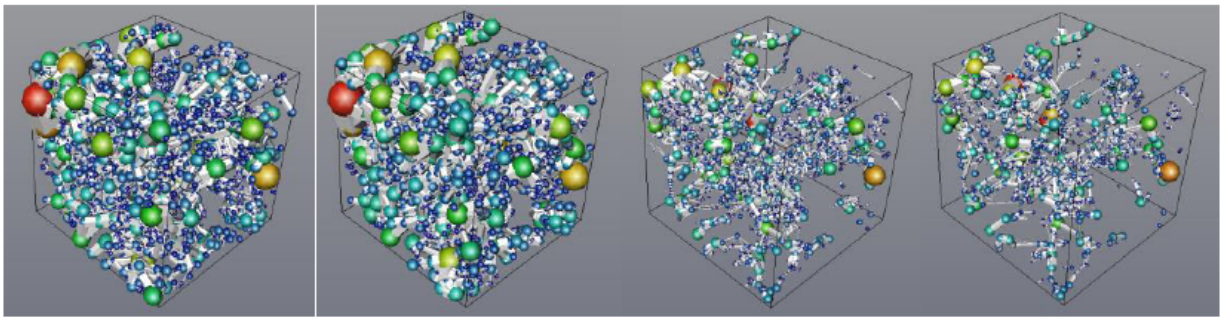

Figure 15: Pore networks of digital rock models with different porosities

Table 1: The results of processing with structuring elements *B* with different radius

Model	Porosity/%	Permeability /mD	Pore Numbers
C1_3	10.22	14.8	2674
C1_3r	8.21	6.87	1805
C1_13	40.4	8434.1	5446
C1_13r	44.75	13559.4	3656

the permeability lower. This indicates when a large radius is adopted for a sphere structuring element, more details will be erased earlier than using a one-voxel-radius structuring element.

4.4 Method advantage and limitation

Based on the μ-CT image, erosion and dilation operations are adopted to generate different porosities in this study. Other mathematical methods have been used to construct models with different porosities before, including stochastic methods [18, 19], process-based methods [20]. When using these methods, each time of the process, the porosities are different, and so are many other parameters. The pore shape of one model can't be guaranteed to maintain the same way as the others. In this study, operations are based on the same μ-CT image. Therefore, the basic pore structures and distributions of the models are the same. And based on the dissolution process, many researchers have done the numerical study of carbonate dissolution by CO2 and its effect on the transport properties [21–25]. These process-based methods can provide us accurate models with different porosities after the present dissolution stage. In this study, the erosion operation can approximately simulate the corrosion effect, while the dilation operations can restore the matrix before the current status. By using dilation and erosion, both higher and lower porosities can be generated.

However, dilation and erosion operations are used under assumptions, namely: (a) the rock corrosion happens evenly and simultaneously at each direction on each pore surface, and (b) the pore will be corroded no matter it is connected to the primary fluid channel or not. Therefore, these methods have nothing to do with physical properties such as the heterogeneous of minerals and gravity. More studies need to be done in the future.

4.5 Reliability of fractured models

We use the FBM method to model the fractures in carbonate rocks based on μ-CT images. The surfaces of natural fractures in rocks have very high self-correlation and self-affine property. The FBM is a standard self-affine model. By using this method, we can generate a fracture-like rough surface. Zhao *et al.* (2013) [10] applied the FBM method to create fractures in sandstones. And based on the fractured models, the electrical simulations were done. By comparing the simulation results with the experimental results, the FBM method was proved efficient. In this study, we adopt this same method into the carbonate rocks. Because the method is based on mathematics, and it has nothing to do with the rock properties, the usage of the FBM method in carbonate rocks is also workable. The fractured digital rock models can be used in the next step physical simulations.

μ-CT is one common but not the only way to build 3D digital rocks. Because the methods and workflows introduced in this paper are purely based on mathematics, they can also be used in carbonate digital rocks reconstructed in other ways, such as using process-based methods.

5 Conclusions

To generate multi-porosity and fractured digital rock models of carbonate rocks for the physical simulation, the erosion and dilation of mathematical morphology and FBM methods were performed based on a μ-CT image. The main results can be summarized as follows:

(1) Erosion operation is similar to the corrosion process in carbonate rocks. The dilation operation is a reverse to the erosion, which can be used to restore the matrix of the former stages. The pore radius distribution frequency curves show the pore space change in the models during the operations: pores are getting larger and smaller after the erosion and dilation, respectively. In both erosion and dilation operations, the pore numbers decrease because of the pore surface area decreases. The porosity-permeability relation is a power exponential function similar to the experimental results. The structuring element B's radius can affect the operation results.

(2) The fracturing method has been applied in sandstones and proved reliable. Because the method to generate fractures is only based on mathematics and has nothing to do with the rock properties, the usage of the FBM method in carbonate rocks is workable.

(3) The analysis results reveal the digital rock models with different porosities and natural fractures are reasonable. The methods and workflows introduced in this paper can also be used in carbonate digital rocks reconstructed in ways other than μ-CT based images such as using process-based methods. The models we build in this research can be used in the next physical simulations. However, the mathematical morphological methods are used based on assumptions of equal corrosion of each pore. Factors such as heterogeneity of minerals and gravity need to be considered in future studies.

Acknowledgement: This research is supported by National Natural Science Foundation of China (grant no. 41504094 and 51704033) and the National Science and Technology Major Project (No. 2017ZX05032003-005). We thank Imperial College for the carbonate digital rock sample. We thank four anonymous reviewers for their constructive suggestions for improvements to the manuscript.

References

[1] Mazzullo, S.J., Chilingarian, G. V, Chapter 4 Diagenesis and Origin of Porosity. In *Carbonate Reservoir Characterization: A Geologic-engineering Analysis, Part I*; Chilingarian, G. V, Mazzullo, S.J., Rieke, H.H.B.T.-D. in P.S., Eds.; Elsevier, 1992; Vol. 30, pp. 199–270 ISBN 0376-7361

[2] Choquette, P.W., Pray, L.C., Geologic nomenclature and classification of porosity in sedimentary carbonates. Am. Assoc. Pet. Geol. Bull. 1970, 54, 207 LP – 244

[3] Arns, C.H., Bauget, F., Limaye, A., Sakellariou, A., Senden, T., Sheppard, A., *et al.*, Pore-Scale Characterization of Carbonates Using X-Ray Microtomography. SPE J. 2005, 10, 26–29

[4] Arns, C.H., Knackstedt, M.A., Pinczewski, W.V., Martys, N.S., Virtual permeametry on microtomographic images. J. Pet. Sci. Eng. 2004, 45, 41–46

[5] Arns, J.Y., Arns, C.H., Sheppard, A.P., Sok, R.M., Knackstedt, M.A., Pinczewski, W.V., Relative permeability from tomographic images; effect of correlated heterogeneity. J. Pet. Sci. Eng. 2003, 39, 247–259

[6] Bakke, S., Øren, P.-E., 3-D Pore-Scale Modelling of Sandstones and Flow Simulations in the Pore Networks. SPE J. 1997, 2, 136–149

[7] Blunt, M.J., Jackson, M.D., Piri, M., Valvatne, P.H., Detailed physics, predictive capabilities and macroscopic consequences for pore-network models of multiphase flow. Adv. Water Resour. 2002, 25, 1069–1089

[8] Zhao, X., Blunt, M.J., Yao, J., Pore-scale modeling: Effects of wettability on waterflood oil recovery. J. Pet. Sci. Eng. 2010, 71, 169–178

[9] Jiang, L., Sun, J., Liu, X., Wang, H., Study of different factors affecting the electrical properties of natural gas reservoir rocks based on digital cores. J. Geophys. Eng. 2011, 8, 366–371

[10] Zhao, J., Sun, J., Liu, X., Chen, H., Cui, L., Numerical simulation of the electrical properties of fractured rock based on digital rock technology. J. Geophys. Eng. 2013, 10, 055009

[11] Sun, J., Zhao, J., Liu, X., Chen, H., Jiang, L., Zhang, J., Pore-scale analysis of electrical properties in thinly bedded rock using digital rock physics. J. Geophys. Eng. 2014, 11, 055008

[12] Wei, Y., Nie, X., Jin, L., Zhang, C., Zhang, C., Zhang, Z., Investigation of sensitivity of shale elastic properties to rock components based on a digital core technology and finite element method. Arab. J. Geosci. 2018, 11, 224

[13] Nie, X., Zou, C., Li, Z., Meng, X., Qi, X., Numerical simulation of the electrical properties of shale gas reservoir rock based on digital core. J. Geophys. Eng. 2016, 13, 481–490

[14] Saxena, N., Mavko, G., Estimating elastic moduli of rocks from thin sections: Digital rock study of 3D properties from 2D images. Comput. Geosci. 2016, 88, 9–21

[15] Knackstedt, M.A., Latham, S., Madadi, M., Sheppard, A., Varslot, T., Arns, C., Digital rock physics: 3D imaging of core material and correlations to acoustic and flow properties. Lead. Edge 2009, 28, 28–33

[16] Yan, W., Sun, J., Zhang, J., Yuan, W., Zhang, L., Cui, L., et al., Studies of electrical properties of low-resistivity sandstones based on digital rock technology. J. Geophys. Eng. 2018, 15, 153–163

[17] Andrä, H., Combaret, N., Dvorkin, J., Glatt, E., Han, J., Kabel, M., *et al.*, Digital rock physics benchmarks-part II: Computing effective properties. Comput. Geosci. 2013, 50, 33–43

[18] Okabe, H., Blunt, M.J., Pore space reconstruction using multiple-point statistics. J. Pet. Sci. Eng. 2005, 46, 121–137
[19] Wu, K., Van Dijke, M.I.J., Couples, G.D., Jiang, Z., Ma, J., Sorbie, K.S., *et al.*, 3D stochastic modelling of heterogeneous porous media - Applications to reservoir rocks. Transp. Porous Media 2006, 65, 443–467
[20] Liu, X., Sun, J., Wang, H., Reconstruction of 3-D digital cores using a hybrid method. Appl. Geophys. 2009, 6, 105–112
[21] Miller, K., Vanorio, T., Keehm, Y., Evolution of permeability and microstructure of tight carbonates due to numerical simulation of calcite dissolution. J. Geophys. Res. Solid Earth 2017, 122, 4460–4474
[22] Nunes, J.P.P., Blunt, M.J., Bijeljic, B., Pore-scale simulation of carbonate dissolution in micro-CT images. J. Geophys. Res. Solid Earth 2016
[23] Hao, Y., Smith, M., Sholokhova, Y., Carroll, S., CO2-induced dissolution of low permeability carbonates. Part II: Numerical modeling of experiments. Adv. Water Resour. 2013, 62, 388–408
[24] Yoon, H., Valocchi, A.J., Werth, C.J., Dewers, T., Pore-scale simulation of mixing-induced calcium carbonate precipitation and dissolution in a microfluidic pore network. Water Resour. Res. 2012, 48, 1–11
[25] Bouchelaghem, F., A numerical and analytical study on calcite dissolution and gypsum precipitation. Appl. Math. Model. 2010, 34, 467–480
[26] Haralick, R.M., Sternberg, S.R., Zhuang, X., Image Analysis Using Mathematical Morphology. IEEE Trans. Pattern Anal. Mach. Intell. 1987, PAMI-9, 532–550
[27] Liu, X., Sun, J., Wang, H., Numerical simulation of rock electrical properties based on digital cores. Appl. Geophys. 2009, 6, 1–7
[28] Odling, N.E., Natural fracture profiles, fractal dimension and joint roughness coefficients. Rock Mech. Rock Eng. 1994, 27, 135–153
[29] Auradou, H., Hulin, J.P., Roux, S., Experimental study of miscible displacement fronts in rough self-affine fractures. Phys. Rev. E - Stat. Nonlinear, Soft Matter Phys. 2001, 63, 066306/1-066306/10
[30] Lu, S., Molz, F.J., Liu, H.H., An efficient, three-dimensional, anisotropic, fractional Brownian motion and truncated fractional Levy motion simulation algorithm based on successive random additions. Comput. Geosci. 2003, 29, 15–25
[31] Kim, T.H., Schechter, D.S., Estimation of Fracture Porosity of Naturally Fractured Reservoirs With No Matrix Porosity Using Fractal Discrete Fracture Networks. SPE Reserv. Eval. Eng. 2009, 12, SPE-110720-PA
[32] Dong, H., Micro-CT imaging and pore network extraction, Imperial College London, 2007
[33] Rashid, F., Glover, P.W.J., Lorinczi, P., Collier, R., Lawrence, J., Porosity and permeability of tight carbonate reservoir rocks in the north of Iraq. J. Pet. Sci. Eng. 2015, 133, 147–161
[34] Valvatne, P.H., Blunt, M.J., Predictive pore-scale modeling of two-phase flow in mixed wet media. Water Resour. Res. 2004, 40, 1–21